Vol. 19, No. 2 (2020) 941-952
Revista Mexicana de Ingeniería Química

Synthesis of Au-TiO_2 nanoparticles as sensors of 3-mercaptopropionic acid

Síntesis de nanopartículas de TiO_2-Au como sensor de ácido 3-mercaptopropiónico

K. Montoya-Villegas[1], R. M. Félix-Navarro[2], L. Rejón-García[3], C. Silva-Carrillo[2], B. Trujillo-Navarrete[1], S. W. Lin-Ho[2], E. A. Reynoso-Soto[1,2*]

[1]*Posgrado en Ciencias de la Ingeniería, Tecnológico Nacional de México/Instituto Tecnológico de Tijuana. A. P. 1166. Tijuana, B. C. 22000, México.*
[2]*Centro de Graduados e Investigación, Tecnológico Nacional de México/Instituto Tecnológico de Tijuana. A. P. 1166. Tijuana, B. C. 22000, México.*
[3]*Instituto Nacional de Electricidad y Energías Limpias, Reforma 113, Palmira, Morelos. C.P. 62490, México.*

Received: August 17, 2019; Accepted: November 4, 2019

Abstract

3-Mercaptopropionic acid (3MPA) is an essential organic compound in aquatic environments since it has a fundamental role in the biogeochemistry of sulfur (S), it is generated during the degradation of sulfur-containing amino acids, such as methionine in some plants and sequential demethylation of dimethylsulfoniopropionate (DMSP). The concentration level of 3MPA in aquatic environments is from nanomolar to micromolar. Besides, 3MPA is toxic at certain concentrations and is used in experimentation to cause seizures in mice for scientific advances in epilepsy. Therefore, in this work, we report the developed of a novel portable, selective, and rapid response sensor; based on an Au-TiO_2 electrode for the quantification of 3MPA. The electrochemical cyclic voltammetry technique was used to obtain the sensor calibration curve, with a limit of detection (LOD) of 50 nM in a linear range of 0 to 80 μM.

Keywords: 3-mercaptopropionic acid, detection, gold nanoparticles, titanium dioxide.

Resumen

El ácido 3-mercaptopropiónico (3MPA) es un compuesto orgánico esencial en ambientes acuáticos dado que tiene un papel fundamental en la biogeoquímica del azufre (S), se genera durante la degradación de aminoácidos que contienen S, como la metionina en algunas plantas y la desmetilación secuencial de dimetilsulfoniopropionato (DMSP). El nivel de concentración del 3MPA en ambientes acuáticos es de nanomolar a micromolar. Además, 3MPA es tóxico a ciertas concentraciones y se usa en experimentación para causar convulsiones en ratones para avances científicos en epilepsia. Por lo tanto, en este trabajo, reportamos el desarrollo de un novedoso sensor portátil, selectivo y de respuesta rápida; basado en un electrodo de TiO_2-Au para la cuantificación de 3MPA. La técnica electroquímica de voltametría cíclica se utilizó para obtener la curva de calibración del sensor, con un límite de detección (LOD) de 50 nM en un rango lineal de 0 a 80 μM.

Palabras clave: ácido 3-mercaptopropiónico, detección, nanopartículas de oro, dióxido de titanio.

1 Introduction

Titanium dioxide (TiO_2) has been studied in various fields for its low cost, abundance in nature, biocompatibility, stable chemical properties, and non-toxicity. Recent research uses TiO_2 in packaging materials because of its antibacterial activity as in the work of Estrada *et al*. (2016), as a catalyst in the work of Cruz *et al*. (2017) and for energy storage systems as in the work of Moya *et al*. (2020). Also, Gonzalez *et al*. (2019) have reported a simple way to improve the dispersion of TiO_2 particles inside chitosan/potato-starch films by chemical modification of the surface of these nanoparticles via silanization.

Sulfur is one of the most plentiful elements on Earth, just as the sulfate ion is one of the most abundant ions (Loka *et al*., 2008). Also, the compounds of S govern the compositions of the oceans and the redox balance on the surface of the Earth. Likewise, lake sediments are typically enriched in sulfur (S) (0.3 - 64 mg/g), compared to materials

* *Corresponding author. E-mail*: edgar.alonso@tectijuana.mx
https://doi.org/10.24275/rmiq/IA800
issn-e: 2395-8472

from the earth's crust (0.03 - 2.7 mg/g) and surface soils (0.05 - 2 mg/g). Although marine sediments have a higher sulfur content and a higher S: C ratio than lacustrine sediments (Jain *et al*., 2006; Herszage, 2001).

Among the compounds containing S are thiols, especially low molecular weight thiols are essential due to their biological rotation in natural environments. They have a fundamental role in the biogeochemistry of S since they are essential intermediaries in the processes involved in the transformation of microbial organic sulfides. Therefore, these characteristics have led to considerable interest in thiol compounds such as cysteine (CySH) and glutathione (GSH), which have critical functions in physiological processes in a variety of living organisms, from microbes to humans (Salgado *et al*., 2015; Mopper *et al*., 1986; Belcastro *et al*., 2004).

There are investigations focused on the detection of thiols. As the work of Kong *et al*., they report a rapid and ecological strategy for the detection of thiol content (n-dodecyl mercaptan, n-$C_{12}H_{25}SH$) in fossil fuels by the cyclic voltammetric method, using a bismuth film electrode in situ (BiFE) with an acetic acid-acetate/methanol electrolyte (Kong *et al*., 2016).

However, less attention has been paid to other low molecular weight hydrophilic thiols, such as 3-mercaptopropionic acid ($HSCH_2CH_2CO_2H$; 3MPA). 3MPA is an essential thiol in natural aquatic environments, is found in nanomolar to micromolar concentrations. Also, 3MPA is toxic at specific concentrations and is an inhibitor of glutamate decarboxylase, which causes a decrease in the concentration of γ-aminobutyric acid (GABA) in the brain, thereby causing seizures. For this reason, the 3MPA is widely used in the experimentation with mice for scientific advances on epilepsy. The detection of 3MPA and its subsequent quantification in different matrices is difficult due to its extreme reactivity (Salgado *et al*., 2015; Vairavamurthy *et al*., 1987; Enrique *et al*., 2017).

Revermann *et al*. (2007) report a method based on microchip capillary electrophoresis (CE) with fluorescence detection for the quantification of thiols in depilatory creams and lotions for permanents. They used the 3MPA as a standard and obtained a detection limit (LOD) of 2 μM (Henry, 2006). Another method of detection is that reported by Salgado *et al*. (2015) by High-Performance Liquid Chromatography (HPLC) with fluorescence detection, in which they use a pre-column derivation with monobromobimane and analysis, for the determination of 3MPA, with a LOD of 4.3 nM.

In this work, we report a novel Au-TiO_2 electrode for the quantification of 3MPA by the electrochemical technique of cyclic voltammetry (CV). In which a system of three electrodes was used; Pt counter electrode, Ag/AgCl reference electrode, and working electrode designed with Au-TiO_2, in phosphate-buffered saline electrolyte for pH 7.

2 Materials and methods

2.1 Materials

All chemical reagents were purchased from Sigma-Aldrich and were used without further treatment. Acetic acid ($C_2H_4O_2$), hydrogen tetrachloroaurate (III) ($HAuCl_4$ $3H_2O$), sodium citrate ($C_6H_5Na_3O_7$ $2H_2O$), ethanol (C_2H_5OH), ethyl-cellulose type 1 (Viscosity of 30-70 mPa.s, 5% in toluene/ethanol 80:20), ethyl-cellulose type 2 (Viscosity of 7-15 mPa.s, 6% in toluene/ethanol 80:20), potassium ferricyanide ($C_6FeK_4N_6$ $3H_2O$), monobasic potassium phosphate (KH_2PO4), dibasic potassium phosphate (K_2HPO_4), heptane (C_7H_{16}), hexanol ($C_6H_{14}O$), isopropanol (C_3H_8O), terpineol ($C_{10}H_{18}O$), titanium isopropoxide (IV) ($C_{12}H_{28}O_4Ti$) and Triton X-100 ($C_{14}H_{22}O(C_2H_4O)_n$(n=9-10)). All aqueous solutions were prepared with MilliQ water (18 m?, Thermo scientific). Transparent conductive substrate (TCO30-10/Li (10 Ohms)) was acquired from Solaronix.

2.2 Synthesis of Au NP by chemical reduction

Gold nanoparticles (Au NP) with spherical morphology were synthesized according to the citrate reduction methodology reported by Frens (1973). An aqueous solution of $HAuCl_4$ $3H_2O$ at 0.1 mol L^{-1} in 25 mL of H_2O was prepared. After that, 75 μL of the $HAuCl_4$ $3H_2O$ solution in 30 mL of H_2O was placed under stirring to obtain a concentration of 0.25 mmol L^{-1}. The solution is heated until boiling, and finally, 900 μL of 1% w/v aqueous sodium citrate solution was added. The solution was allowed to react under mechanical stirring until the solution change to red (Li *et al*., 2011). Subsequently, the fresh prepare Au NP solution was purified by centrifugation at 12973 RCF for 30 min. Then, the residue is dispersed in

water, and the supernatant was further centrifuged to recover a little more Au NP. For the storage of Au NP, they should be protected from the light because they are sensitive to it. In addition, they were cooled, and before any measurement, were equilibrated at room temperature (Balasubramanian *et al*., 2010).

2.3 Synthesis of titanium dioxide nanoparticles by solvothermal method

Nanoparticles of mesoporous titanium dioxide (TiO_2) were synthesized according to the procedure reported by Li *et al*. (2014) with minor modifications. First, the microemulsion solution was prepared into a 100 mL Teflon autoclave by adding 6.62 mmol of heptane, 2.63 mmol of hexanol, 16.54 mmol of Triton X-100, and 0.48 mol of deionized H_2O. The microemulsion solution was left under magnetic stirring for 10 min and was added 6.59 mmol of titanium isopropoxide (TIP), dropwise. After that, the autoclave was placed in an oven for solvothermal treatment at 150 ºC for 13 h. Subsequently, the autoclave was cooled naturally to room temperature, and the precipitate was filtered and washed with water and ethanol. Then, the white solid was allowed to dry for 20 min at 100 °C. Finally, it was given thermal treatment at 250 °C for 3 h at 3 °C min^{-1} to remove residual surfactant molecules of the mesoporous TiO_2 nanoparticles.

2.4 Impregnation of gold nanoparticles (Au NP) over mesoporous TiO_2 nanoparticles

On the other hand, Au NP was incorporated into the mesoporous TiO_2 nanoparticles by the wet impregnation procedure as following: 500 mg of the mesoporous TiO_2 nanoparticle powder was mixed with the appropriate amount of the Au NP aqueous solution, depending on the desired gold concentration of 0.10%, 0.50%, 0.75% and 1.00% in atomic weight. In this case, four samples were obtained and labeled as Au-Ti1, Au-Ti2, Au-Ti3, and Au-Ti4, and correspond to 0.10%, 0.50%, 0.75%, and 1.00% respectively. The samples were allowed to warm in constant agitation until the mesoporous TiO_2 nanoparticles powders impregned with Au NP were dry.

2.5 Preparation of Ti and Au-Ti inks for electrode modification

In order to modify the TCO glass with Ti or Au-Ti samples, the corresponding samples inks were prepared. First, ethyl cellulose (1 and 2) were mixed and appropriately dissolved in isopropanol, mixing 300 mg of each to obtain a 20% w/v solution (Ito *et al*., 2007). After that, the Ti or Au-Ti samples are put into agate mortar and mill with 1 mL of acetic acid grinding for 5 min; and then add 1 mL of H_2O and continue ground for 1 min repeating this step 5 times. In addition to this step, add 1 mL of isopropanol 15 times with constant grinding. After that, the Ti and Au-Ti pastes were transferred to a glass vial and stirred for 1 minute and subjected to ultrasound for two seconds, repeating this procedure 30 times. To the following were added 0.012 mol of terpineol and allowed to stir for 1 min. Finally, the pastes were mixed with the ethylcellulose solution and stirred for 1 min and subjected to ultrasound for two seconds, repeating this procedure 30 times. Then, isopropanol was evaporated to obtain the corresponding inks.

2.6 Characterization of materials

The physicochemical characterization of the synthesized materials was carried out through several techniques: The surface plasmon of the Au NP was analyzed by visible, ultraviolet spectroscopy (UV-VIS) with the rayleigh UV-2601 instrument. Particle size and polydispersity were determined by dynamic light scattering (DLS) with the ZetaSizer (Nano-ZS) nano series from Malvern Instruments, specifying refractive index and absorption of NP-Au, 0.2 and 3.320 respectively. The concentration of the synthesized Au NP was obtained by inductive coupling plasma spectrometry (ICP) with the Optima 8300 Optical Emission Spectrometer from PerkinElmer. The morphology, size distribution, and dispersion of the Au and TiO_2 nanoparticles were observed by field emission scanning electron microscopy (FESEM) using the JSM7800F JEOL microscope. Also, the morphology of the Au-TiO_2 powders was observed by scanning transmission electron microscopy (STEM) with the JEOL 2200Fs+Cs microscope with a spherical aberration corrector. The crystal structure of TiO_2 was analyzed by Raman spectroscopy with the Raman DXR SmartRaman spectroscope from Thermo Scientific with a 780 nm wavelength laser; also, by X-ray diffraction with the Xpert-Pro MPD X-ray diffractometer, PANalytical Ltd. In Bragg-Brentano geometry with Cu Kα = 0.15406 nm radiation. The thermal stability of TiO_2 was studied by thermogravimetric analysis (TGA). The bandgap of materials was obtained by diffuse reflectance with

UV-VIS equipment coupled with a diffuse reflectance integration sphere.

The electrochemical characterization was carried out by cyclic voltammetry (CV). The detection tests of the 3MPA and other analytes of interest, were made using the VMP-300 equipment from BioLogic Science Instruments. The experiment were carried out in a conventional three-electrode system: the TCO glass with the deposited film of active material as the working electrode, the platinum (Pt) counter electrode and the Ag/AgCl reference electrode; in phosphate buffer saline (PBS) for pH 7.

3 Results and discussion

3.1 Characterization of gold nanoparticles

In Fig 1, are shown the different characterization made in order to identify the formation and concentration of Au NP. Fig 1a shows the UV-Vis absorption spectrum characteristic of Au NP presenting the surface plasmon band at 520 nm, which correspond to spherical particles as reported by several authors (Sandu, 2012; Panigrahi *et al.*, 2007). The shape of the surface plasmon band of Au NP indicates a narrow size distribution confirmed by the full width at half maximum (FWHM) of 60.99 nm (Oliveira *et al.*, 2017). In addition, the particle size and concentration were estimated from the absorption spectrum of Au NP, as reported by Haiss *et al*. with Ecs. (1) moreover, (2) (Haiss *et al*., 2007).

$$d = \exp\left(B_1 \frac{A_{spr}}{A_{450}} - B_2\right) \tag{1}$$

Where, d is the diameter (in nm), B_1 and B_2 are determined constants (B_1 = 3.55; B_2 = 3.11), A_{spr} is the surface plasmon resonance peak, and A_{450} is the absorbance at 450 nm.

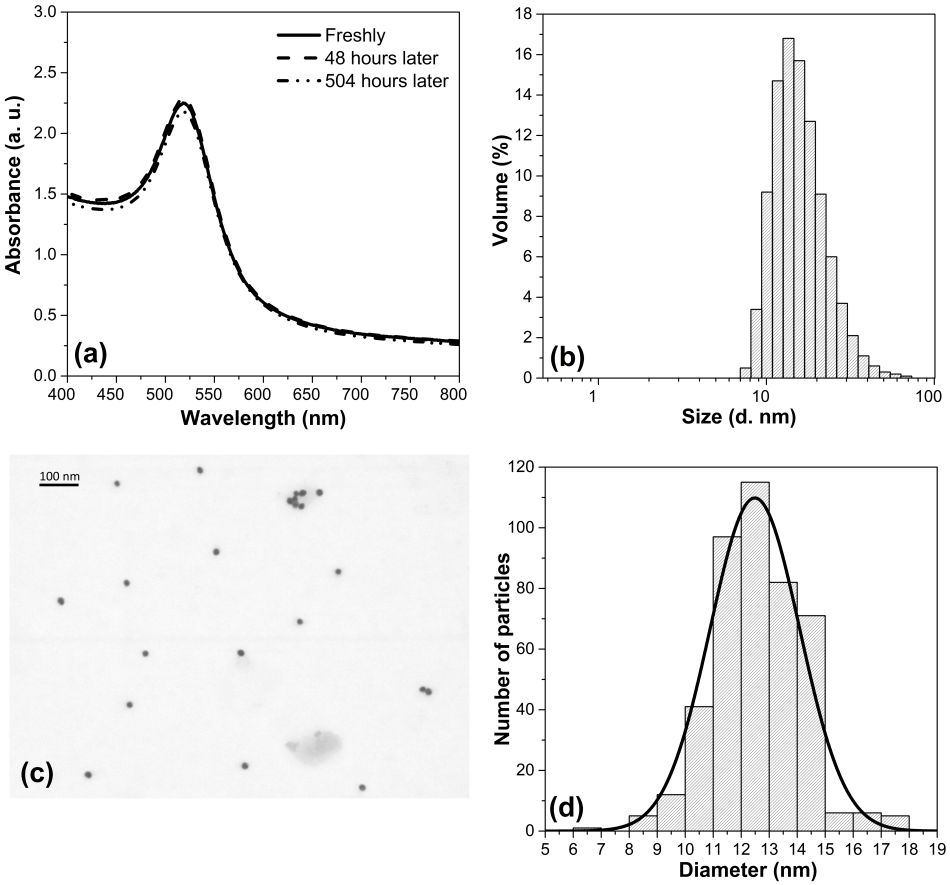

Fig. 1. Characterizations of gold particles (a) UV/VIS spectrum, (b) DLS size distribution, (c) STEM micrograph, (d) Size distribution from STEM measurements.

$$d = \left(\frac{A_{spr}(5.89 \times 10^{-6}}{C_{Au} \exp(C_1)} \right)^{1/C_2} \quad (2)$$

Where C_{Au} is Au concentration (in mol/L), C_1 and C_2 are determined constants (C_1 = -4.75; C_2 = 0.314) (Haiss *et al*., 2007). From these equations with the UV-Vis absorption spectrum of Au NP, the particle diameter ad concentration were estimated, and the result was 11.70 nm and 142 ppm, respectively. In order to confirm the diameter and concentration of Au NP, the DLS and ICP measurements were made as shown in Figure 1b; the results of DLS show a hydrodynamic diameter of 16.97 ± 7.80 nm with a polydispersity of 0.591, and the concentration was of 141.89 ppm obtained by ICP measurement. The morphology and size of the Au particles were determined by the STEM mode characterization as shown in Figure 1c and 1d, confirming that the gold particles have a spherical morphology with a particle size distribution of 12.49 ± 1.60 nm, and the results are consistent with the different techniques used in the characterization of the Au NP solution.

3.2 Characterization of TiO_2 nanoparticles

Several techniques were employed in the characterization of TiO_2 nanoparticles to determine the crystalline structure, morphology, and nanoparticles size, as shown in Fig 2. In the Raman spectra of Fig 2a, four Raman modes are observed and correspond to the active modes of anatase crystal at 146.46 (Eg (1)), 399.09 (B_{1g}), 516.08 (A_{1g}) and 640.07 cm^{-1} (E_g (2)); and the Raman mode of (Eg (1)) presents an FWHM of 21.88 cm^{-1} attributed to nanoparticles of 20 nm approximately (Choi *et al*., 2005; Pérez *et al*. 2019).

Furthermore, the XRD patterns of the powder materials are shown in Fig 2b. The peaks are well defined and are identified to the corresponding (101), (110), (004), (200), (105), (211), (204), (116), (220) and (215) crystal planes. Most can be correctly assigned to the anatase phase except one, the peak (110); this peak is assigned to the rutile phase (Wei *et al*., 2013; Nuansing *et al*., 2006). Therefore these TiO_2 materials have 90.43% of anatase phase and 9.57% of the rutile phase, and these data were calculated with Eq. (3).

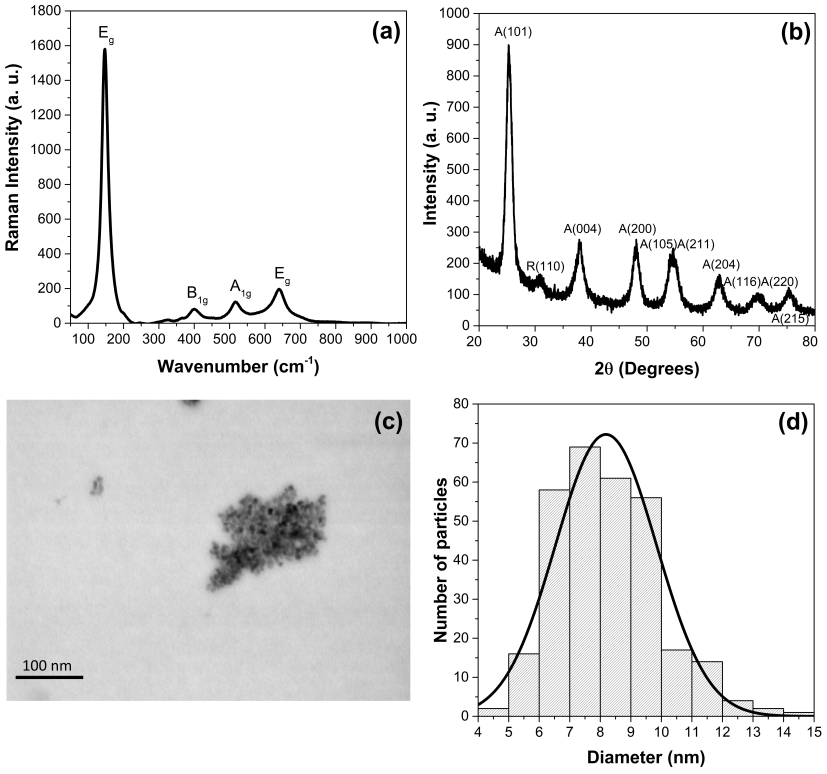

Figure 2. Characterizations of TiO_2 nanoparticles (a) Raman spectrum, (b) XRD spectrum, (c) STEM micrograph, (d) Size distribution from FE-SEM.

$$F_R = \frac{1}{1 + 1.26\frac{I_A(101)}{I_R(110)}} \quad (3)$$

Where F_R is the percentage content of the rutile phase, $I_A(101)$ and $I_R(110)$ are the integral (101) intensities of anatase phase and (110) of the rutile phase, respectively (Nuansing *et al*., 2006). Also, from the XRD spectrum of TiO_2 powders was estimate the particle size by the Eq. (4) reported by Zhang *et al*. (2003).

$$D = \frac{K\lambda}{\beta\cos\theta} \quad (4)$$

Where D is the average crystallite size in angstrom, K is the Scherrer constant that is taken as 0.94, λ is the wavelength of the X-ray radiation (Cu Kα, 0.15406 nm), β is the FWHM, and θ is the diffraction angle (Zhang *et al*., 2003; Ibrahim *et al*. 2017). The particle size of TiO_2 from XRD was 6.99 nm. In order to confirm the diameter of TiO_2 nanoparticles and morphology was characterized by STEM, as shown in Fig 2c and Fig 2d, confirming that TiO_2 nanoparticles present polygonal or almost spherical morphology with a nanoparticle size distribution of 8.19 ± 1.66 nm, and the result is consistent with the XRD characterization technique of TiO_2 nanoparticles.

Also, the thermal analysis of the TiO_2 powders is presented in Fig 3. The curve depicted a weight loss at 60 °C, which indicates the desorption of ethanol. Also, can be appreciated a second weight loss at 120 °C attributed to water desorption, and finally are present other two-weight losses at 217 °C and 538 °C, these losses were attributed to the gradual decomposition of Triton X-100, and anatase-rutile phase transformation - obtaining ~94% of TiO_2 residue (Nuansing *et al*., 2006; Mallick *et al*., 2018).

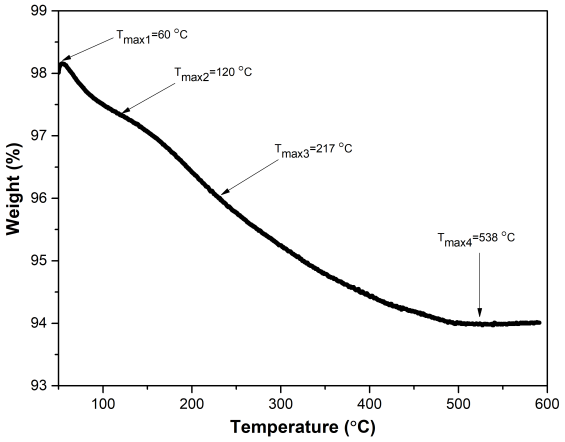

Figure 3. Thermogram of TiO_2 nanoparticles.

3.3 Characterization of Au-TiO_2 nanoparticles

Mesoporous TiO_2 nanoparticles powders were decorated with different gold concentrations of 0.10%, 0.50%, 0.75% and 1.00% at. The TiO_2 powders with Au NP were characterized by STEM, as shown in Fig 4., can be observed the TiO_2 nanoparticles well dispersed and compare with the Au-TiO_2 micrograph in Fig 4b; in which the decoration of Au NP can be appreciated as little spheres with major contrast over the surface of TiO_2 nanoparticles. Also, the Au-TiO_2 was characterized based on the diffuse reflectance technique, as shown in the Fig 4c. To measure the bandgap of each material. The Tauc diagram of Fig 4d is used for calculating the bandgap (Soto *et al*., 2014):

$$yaxis = (F(R) * hv)^{1/2} \quad (5)$$

where hv is the photon energy, and $F(R)$ is the function that depends on the diffuse reflectance value, this function is expressed as:

$$F(R) = \frac{(1-R)^2}{2R} \quad (6)$$

Fig 4d shows the Tauc diagram based on the diffuse reflectance spectrum of Fig 4c. In which, the pronounced increase in reflectance between 330 and 395 nm can be observed, and with the Tauc diagram they have a band interval of 3.23 eV, characteristic of TiO_2 in the anatase phase (Ibrahim *et al*., 2017). On the other hand, concerning Au1-Ti, it can be inferred that its decoration with Au NP is insignificant under this technique because its prohibited band is equal to that of pure TiO_2. Meanwhile, the other three nanomaterials of TiO_2 have a band different from the corresponding of TiO_2, which is clearly distinguished around 550 nm, as a summary in Table 1. The new band at 550 nm is attributed to surface plasmon resonance of Au NP, which confirms the existence of Au^0 nanoparticles (Gogoi *et al*., 2018).

Table 1. Band gaps of Au-TiO_2.

Sample	Band Gap (eV)
TiO_2	3.23
Au-Ti1	3.23
Au-Ti2	0.97, 3.23
Au-Ti3	1.89, 3.23
Au-Ti4	1.53, 3.23

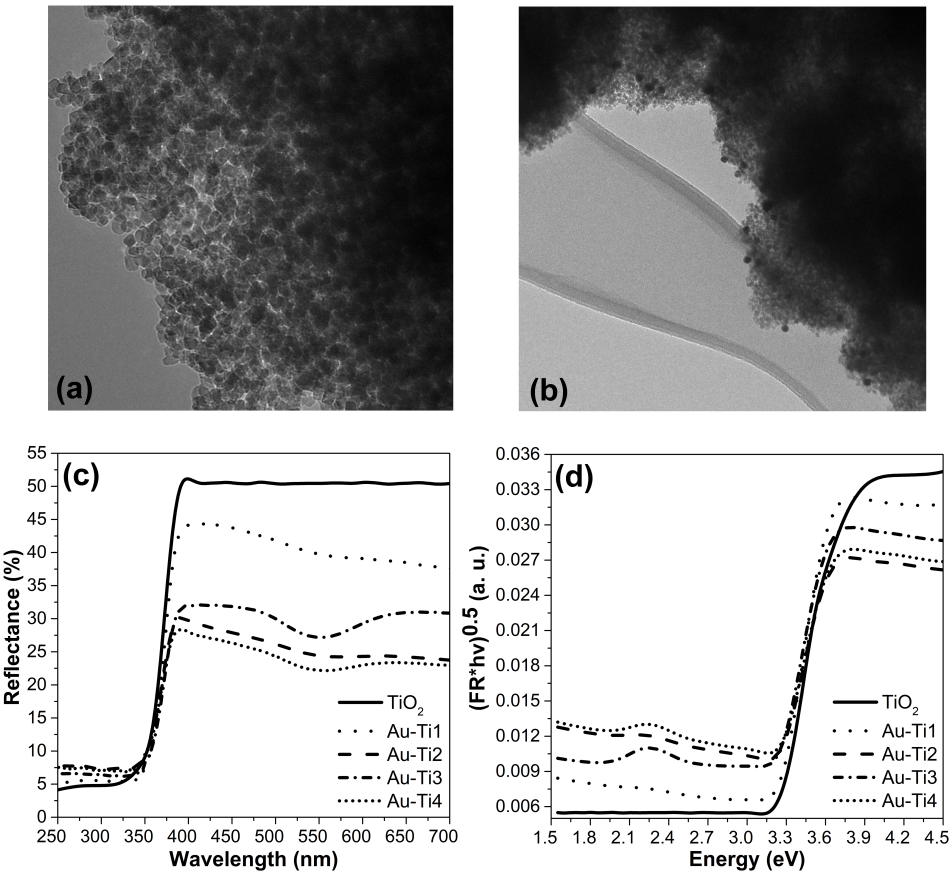

Figure 4. STEM micrographs of (a) TiO_2 and (b) Au-TiO_2. Characterizations of Au-TiO_2 (c) diffuse reflectance spectrum, (d) Tauc plot.

3.4 Electrochemistry of 3MPA at Au-TiO_2 cyclic voltammetric

To evaluate the electrocatalytic activity of the Au-TiO_2 electrodes, this was carried by cyclic voltammetric (CV) obtained in phosphate-buffered saline (PBS to pH 7.0) at 100 mV/s, in the absence and presence of different concentrations of 3MPA (Fig 5a). In these voltammograms, cathodic current is observed at -0.69 V and can be explained in terms of the formation of Ti^{3+} at the upper monolayer of TiO_2 film as reported in literature (Kim *et al*., 2003) anode current is observed at -0.78 V, corresponding to the oxidation of hydrogen that could have been adsorbed or absorbed in the titanium or that a titanium hydride was formed during the cathodic process at -0.69 V (Garcia *et al*., 2014). The catalytic activity of the TiO_2 electrode in the absence of Au NP can be observed by the increase in the current of the cathodic peak, and this can be explained by the reduction of Ti^{3+} sites by the oxidation of thiol groups of 3MPA (Peláez *et al*., 2011). On the other hand, in the electrodes with Au NP, another anodic current was observed at 0.82 V, corresponding to the oxidation of the thiol group on the surface of Au NP and its adsorption on the surface of the Au-TiO_2 electrodes (Rhieu *et al*., 2015).

Therefore, calibration curves were obtained in the oxidation and reduction regions of the CV at 0.82 and -0.69 V vs. Ag/AgCl, where the current increase with the increase of 3MPA concentration. The calibration curves obtained with the Au-TiO_2 electrodes at 0.82 V are shown in Fig. 5b, it is notable that in this potential with the TiO_2 electrode, the anodic current signal was not appreciated as with the electrodes that contain Au NP, and this can be explained because Au NP promotes the oxidation of thiol group to thiolate and adsorb on the surface of Au NP by acid-base Pearson interaction. For the analysis of these data, the sensitivity (slope) and detection limit (LOD) of the electrode for the detection of 3MPA was calculated and is summarized

in Table 2, the LODs were calculated according to the definition $Y_{LOD} = Y_B + 3S_B$ reported in the literature (Miller *et al*., 2000).

It was observed that the sensitivity of the Au-TiO_2 electrodes was improved at a high concentration of Au NP until the concentration of Au was of 1 atomic percent; showing a decrease in the sensitivity. The decrease in sensitivity can be attributed to the agglomeration of Au NP, thus decreasing the surface area for the interaction with the oxidate species of 3MPA thiolate. Therefore, the best Au-TiO_2 electrode for the quantification of 3MPA is the one that contains the 0.75% atomic of Au (Au-Ti3); its calibration curve with the error bars is shown in Fig 5c, which has a sensitivity to 3MPA of 0.224±0.007 μC/ppm and a LOD of 0.005 ppm equal to 50 nM.

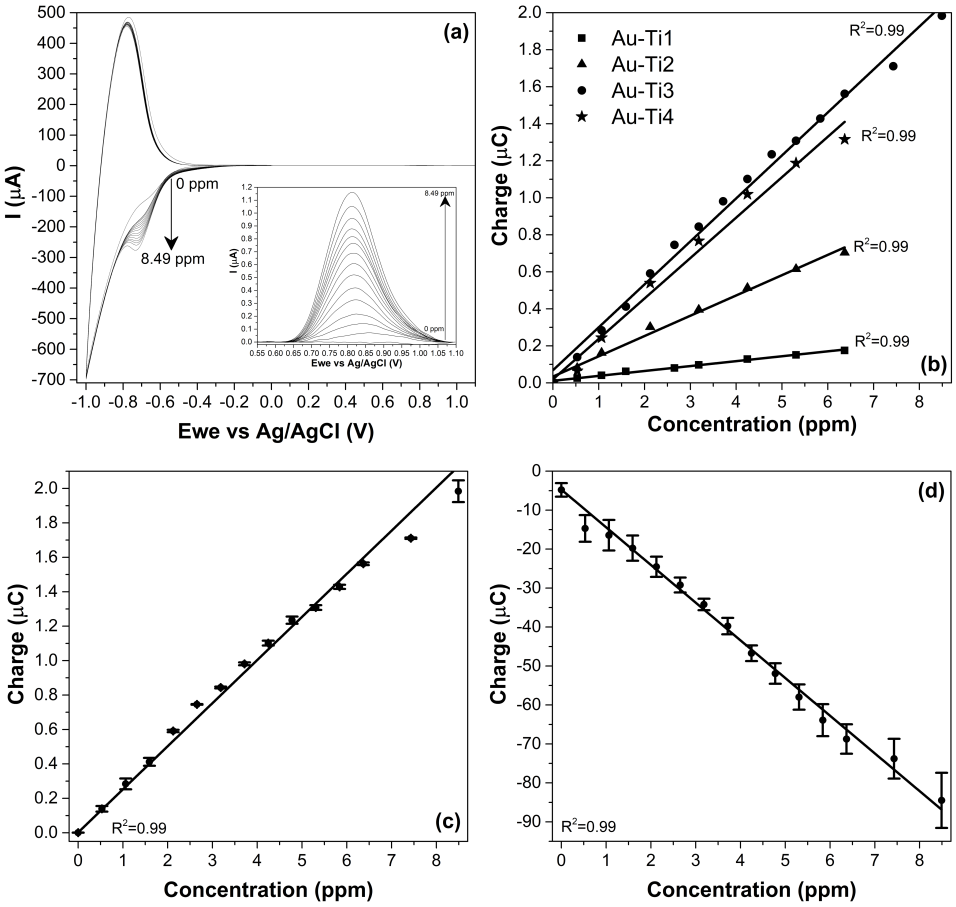

Figure 5. 3MPA detection by (a) cyclic voltammetry. Calibration curves of (b) Au-TiO_2 nanomaterials obtained at 0.82 V, (c) Au-Ti3 at 0.82 V, (d) Au-Ti3 at -0.69 V.

Table 2. Parameters of calibrations curves of the Au-TiO_2 for detection of 3MPA at 0.82 V potential.

Sample	Sensitivity (μC/ppm)	LOD (ppm)	LOD (μM)
Au-Ti1	0.027	0.539	5.10
Au-Ti2	0.110	0.004	0.04
Au-Ti3	0.224	0.005	0.05
Au-Ti4	0.218	0.006	0.06

In the same way, the CV data of the cathodic process at -0.69 V were analyzed, this corresponding to the reduction of Ti^{3+} sites by the 3MPA hydrocarbon chain. The best electrode was Au-Ti3; the calibration curve is shown in Fig 5d, which has a sensitivity of 8.81 ± 2.16 μC/ppm and a LOD of 0.048 ppm equal to 460 nM. These results indicate that the most active and sensitive sites for the detection and quantification of 3MPAis the anodic site when the Au NP is present.

Due to the fact that the 3MPA structure contains a carboxylic and thiol groups, it was analyzed that the sensors based on Au-TiO_2 are sensitive to 3MPA, due to their carboxylic group at the potential of -0.69 V (referred to the reduction of Ti^{3+} sites) or to the thiol group at the 0.82 V potential (referred to the oxidation of thiol to thiolate group).

Therefore, to verify the interactions described above, the sensitivity of the Au-Ti3 electrode to propionic acid (PA) was compared with respect to 3MP; because PA is a molecule similar to 3MPA but without the presence of the thiol group. Figure 6a shows the obtained voltammograms, where the change in the cathodic current can be observed, but when the voltammograms in the range of 0.55 V to 1.10 V were analyzed, the signal attributed to the interaction of the thiol group with the Au NP no appeared.

With the voltammograms obtained from the Au-Ti3 electrode in the presence of PA, the calibration curve of Fig. 6b was obtained, with a sensitivity of 2.55 μC / ppm and a LOD of 0.13 ppm, which is equal to 1.22 μM. When comparing these data from the Ti-Au3 electrode to the AP with those obtained for 3MPA in the cathodic potential, it was observed that the sensitivity decreased, and the LOD increased dramatically with respect to that shown for the PA. The change in sensitivity and LOD of the Au-Ti3 electrode in the presence of 3MPA can be attributed to the thiol group in 3MPA, which could catalyze the reduction reaction of Ti^{3+} with the 3MPA hydrocarbon chain.

Conclusions

In this study, a new sensor based on Au-TiO_2 was developed for the detection and electrochemical quantification of 3MPA. The presence of Au NP allows the selective oxidation of the thiol group of 3MPA, in a concentration range of 0 to 9 ppm, with high sensitivity 0.224 ± 0.007 μC / ppm and a low LOD of 50 nM. This sensor has the potential to be used in the detection of 3MPA in future studies on seawater samples.

Acknowledgements

The authors thank Tijuana Technological Institute for providing the facilities for this research. K. Montoya-Villegas wishes to thank CONACyT for the doctoral scholarship. Also, the authors thank CONACyT and TecNM for financial assistance through the projects PN-2015-92, and 5273.19-P respectively. Thanks are due to Nanotechnology National Lab, located at CIMAV, Chihuahua, Mexico, for electron microscopy and X-ray diffraction study. The authors thank S. Perez, F. Paraguay, C. Ornelas and R. Salinas for their technical help.

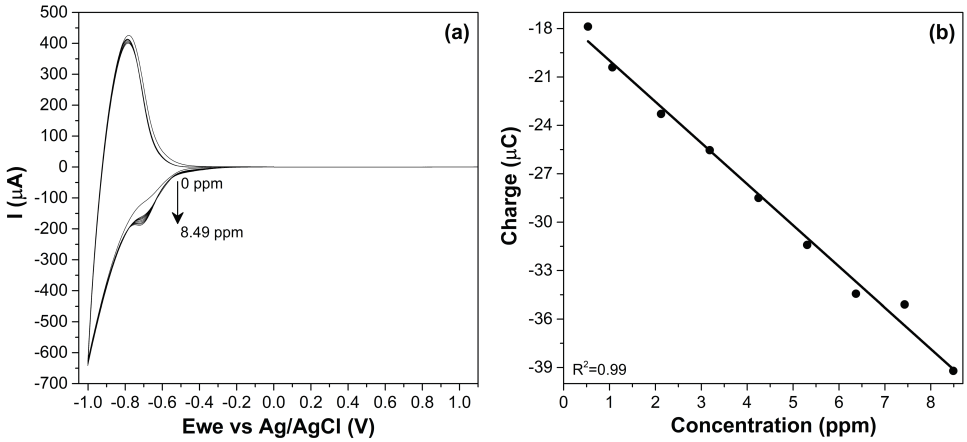

Figure 6. PA detection by (a) cyclic voltammetry and (b) calibration curve of Au-Ti3 at -0.69 V.

References

Balasubramanian, S. K., Yang, L., Yung, Y. L., Ong, C.N., Ong, W.Y., Yu, L. E. (2010). Characterization, purification, and stability of gold nanoparticles. *Biomaterials 31*, 9023-9030. https://doi.org/10.1016/j.biomaterials.2010.08.012

Belcastro, M., Marino, T., Russo, N., Sicilia, E. (2004). Structure and coordination modes in the interaction between Cd^{2+} and 3-mercaptopropionic acid. *The Journal of Physical Chemistry A 108*, 8407-8410. https://doi.org/10.1021/jp047867u

Choi, H. C., Jung, Y. M., Kim, S. B. (2005). Size effects in the Raman spectra of TiO_2 nanoparticles. *Vib. Spectrosc 37*, 33-38. https://doi.org/10.1016/j.vibspec.2004.05.006

Cruz-Ortiz, B.R., Díaz-Jiménez, L., Cortés-Hernández, D.A., Múzquiz-Ramos, E.M. (2017). TiO_2 catalysis used in claus processes: deactivation causes and catalytic activity. *Revista Mexicana de Ingeniería Química 16*, 229-236.

Enrique, A., Goicoechea, S., Castano, R., Taborda, F., Rocha, L., Orozco, S., Girardi, E., Blanch, B. L. (2017). New model of pharmacoresistant seizures induced by 3-mercaptopropionic acid in mice. *Epilepsy Research 129*, 8-16. https://doi.org/10.1016/j.eplepsyres.2016.10.012

Estrada-Monge, A., Andreu-Díaz, J.M., Cruz-Salgado, J. (2016). LDPE/Nano-TiO_2 films with antibacterial properties induced by ultrasound. *Revista Mexicana de Ingeniería Química 15*, 953-960.

Frens, G. (1973). Controlled nucleation for the regulation of the particle size in Monodisperse gold suspensions. *Nature Physical Science 241*, 20-22. https://doi.org/10.1038/physci241020a0

Garcia-Gomez, N. A., Mosqueda, H. A., Garcia-Gutierrez, D. I., Sanchez, E. M. (2014). Electrochemical behavior of TiO_2/carbon dual nanofibers. *Electrochimica Acta 116*, 19-25. https://doi.org/10.1016/j.electacta.2013.10.208

Gogoi, N., Borah, G., Gogoi, P. K., Chetia, T. R. (2018). TiO_2 supported gold nanoparticles: An efficient photocatalyst for oxidation of alcohol to aldehyde and ketone in presence of visible light irradiation. *Chemical Physics Letters 692*, 224-231. https://doi.org/10.1016/j.cplett.2017.12.015

Gonzalez-Calderon, J., Vallejo-Montesinos, J., Martínez-Martínez, H., Cerecero-Enríquez, R., López-Zamora, L. (2019). Effect of chemical modification of titanium dioxide particles via silanization under properties of chitosan/potato-starch films. *Revista Mexicana de Ingeniería Química 18*, 913-927. https://doi.org/10.24275/uam/izt/dcbi/revmexingquim/2019v18n3/GonzalezC

Haiss, W., Thanh, N. T. K., Aveyard, J., Fernig, D. G. (2007). Determination of size and concentration of gold nanoparticles from UV-Vis spectra. *Analytical Chemistry 79*, 4215-4221. https://doi.org/10.1021/ac0702084

Henry, C. (2006). Microchip capillary electrophoresis: An introduction. *Methods in Molecular Biology* (Clifton, N.J.) 1-10. https://doi.org/10.1385/1-59745-076-6:1

Herszage, J. (2001). Oxidación de compuestos sulfurados en presencia de óxidos metálicos de interés en química de medio ambiente. Ph.D. thesis, Universidad de Buenos Aires, Buenos Aires, Argentina.

Ibrahim, A., Mekprasart, W., Pecharapa, W. (2017). Anatase/rutile TiO_2 composite prepared via sonochemical process and their photocatalytic activity. *Materials Today: Proceedings 4*, 6159-6165. https://doi.org/10.1016/j.matpr.2017.06.110

Ito, S., Chen, P., Comte, P., Nazeeruddin, M. K., Liska, P., Péch, P., Grätzel, M. P. (2007). Fabrication of screen-printing pastes from TiO_2 powders for dye-sensitised solar cells. *Progress in Photovoltaics 15*, 603-612. https://doi.org/10.1002/pip.768

Jain, P. K., Lee, K. S., El-Sayed, I. H., El-Sayed, M. A. (2006). Calculated absorption and scattering properties of gold nanoparticles of different

size, shape, and composition: Applications in biological imaging and biomedicine. *The Journal of Physical Chemistry B 110*, 7238-7248. https://doi.org/10.1021/jp057170o

Kim, J.-D., Pyun S. I., Seo, M. (2003). Effect of hydrogen on stresses in anodic oxide film on titanium. *Electrochimica Acta 48*, 1123-1130. https://doi.org/10.1016/S0013-4686(02)00823-X

Kong, D., Kong, W., Khan, Z. U. H., Wan, P., Chen, Y., Yang, M. (2016). Determination of thiol content in fossil fuel by cyclic voltammetry using *in situ* Bismuth film electrode. *Fuel 182*, 266-271. https://doi.org/10.1016/j.fuel.2016.05.093

Li, J., Wu, J., Zhang, X., Liu, Y., Zhou, D., Sun, H., Zhang, H., Yang, B. (2011). Controllable synthesis of stable urchin-like gold nanoparticles using hydroquinone to tune the reactivity of gold chloride. *The Journal of Physical Chemistry C 115*, 3630-3637. https://doi.org/10.1021/jp1119074

Li, X., Zheng, W., He, G., Zhao, R., Lui, D. (2014). Morphology control of TiO_2 nanoparticle in microemulsion and its photocatalytic property. *ACS Sustainable Chemistry & Engineering 2*, 288-295. https://doi.org/10.1021/sc400328u

Loka Bharathi, P. A. (2008) Sulfur cycle. In *Encyclopedia of Ecology* (Second Edition), Fath, B., Ed. Elsevier: Oxford, pp 192-199. https://doi.org/10.1016/B978-0-444-63768-0.00761-7

Mallick, S., Ahmad, Z., Touati, F., Bhadra, J., Shakoor, R. A., Al-Thani, N. J. (2018). PLA-TiO_2 nanocomposites: Thermal, morphological, structural, and humidity sensing properties. *Ceramics International 44*, 16507-16513. https://doi.org/10.1016/j.ceramint.2018.06.068

Miller, J. C.; Miller, J. N., (2000). *Statistics and Chemometrics for Analytical Chemistry*. 4th ed.; Prentice-Hall: Harlow, England; New York. ISBN: 0130228885

Mopper, K.; Taylor, B. F., (1986). Biogeochemical Cycling of Sulfur. In *Organic Marine Geochemistry*, Shon, M., Ed. American Chemical Society: Washington, D.C., United States, pp 324-339. https://doi.org/10.1021/bk-1986-0305.ch019

Moya-Canul, K.M., Yáñez-Limón, J.M. (2020) Study of $Bi_{0.5}NA_{0.5}TiO_3$ system doped with La^{3+} obtained by acetic acid route in sol-gel process. *Revista Mexicana de Ingeniería Química 19*, 335-343. https://doi.org/10.24275/rmiq/Mat591

Nuansing, W., Ninmuang, S., Jarernboon, W., Maensiri, S., Seraphin, S. (2006). Structural characterization and morphology of electrospun TiO_2 nanofibers. *Materials Science and Engineering: B 131*, 147-155. https://doi.org/10.1016/j.mseb.2006.04.030

Panigrahi, S., Basu, S., Praharaj, S., Pande, S., Jana, S., Pal, A., Ghosh, S. K., Pal, T. (2007) Synthesis and size-selective catalysis by supported gold nanoparticles: Study on heterogeneous and homogeneous catalytic process. *The Journal of Physical Chemistry C 111*, 4596-4605. https://doi.org/10.1021/jp067554u

Peláez Abellán, E., Rocha-Souza, L., Guastaldi, A. C. (2011). Cathodic behavior of anodized titanium in simulated physiological. *Latin American Applied Research 41*, 199-203. http://www.laar.plapiqui.edu.ar/OJS/public/site/volumens/indexes/artic_v4103/Vol41_03_199.pdf

Pérez-Osorio, G., Hernández-Aldana, F., Mendoza Hernández, J., Arriola-Morales, J., Castillo-Morales, M., Gutiérrez-Martin, S., Gutiérrez-Arias, J. (2019). Photodegradation of erionyl dye in aqueous medium by sunlight and palladium catalysts. *Revista Mexicana de Ingeniería Química 18*, 1027-1035. https://doi.org/10.24275/uam/izt/dcbi/revmexingquim/2019v18n3/Perez

Revermann, T., Götz, S., Karst, U. (2007). Quantitative analysis of thiols in consumer products on a microfluidic CE chip with fluorescence detection. *Electrophoresis 28*, 1154-1160. https://doi.org/10.1002/elps.200600419

Rhieu, S. Y., Reipa, V. (2015). Tuning the size of gold nanoparticles with repetitive

oxidation-reduction cycles. *American Journal of Nanomaterials 3*, 15-21. https://doi.org/10.12691/ajn-3-1-2

Salgado, P., Visnevschi-Necrasov, T., Kiene, R. P., Azevedo, I., Rocha, A. C. S., Almeida, C. M. R., Magalhães, C. (2015). Determination of 3-mercaptopropionic acid by HPLC: A sensitive method for environmental applications. *Journal of Chromatography B 992*, 103-108. https://doi.org/10.1016/j.jchromb.2015.04.008

Sandu, T. (2012). Shape effects on localized surface plasmon resonances in metallic nanoparticles. *Journal of Nanoparticle Research 14*, 905. https://doi.org/10.1007/s11051-012-0905-6

Soto-Borbón, M.A., Sánchez-Corrales, V.M., Trujillo-Camacho, M.E. (2014). Characterization of TiO_2/alginate screenprinting films. *Revista Mexicana de Ingeniería Química 13*, 227-236.

Vairavamurthy, A., Mopper, K. (1987). Geochemical formation of organosulphur compounds (thiols) by addition of H_2S to sedimentary organic matter. *Nature 329*, 623-625. https://doi.org/10.1038/329623a0

Wei, X., Zhu, G., Fang, J., Chen, J. (2013). Synthesis, characterization, and photocatalysis of well-dispersible phase-pure anatase TiO_2 nanoparticles. *International Journal of Photoenergy 2013*, 1-6. https://doi.org/10.1155/2013/726872

Zhang, Z., Zhou, F., Lavernia, E. J. (2003). On the analysis of grain size in bulk nanocrystalline materials via x-ray diffraction. *Metallurgical and Materials Transactions A 34*, 1349-1355. https://doi.org/10.1007/s11661-003-0246-2